PAPER

Check for updates

3D UV printing with a polymeric ionic liquid and its gold nanoparticle-embedded composites

Susana Ferrufino Amador,[a] Rudy White,[a] Olivia Downey,[a] Kayla Foy,[a] Rachel Wynn,[a] Hawa Khan,[a] Megan O'Neil,[b] Olivia McNair[b] and Samrat Dutta (ID) *[a]

Polymeric ionic liquids are a diverse class of ion-conducting materials with tunable properties that can advance the applicability of additive manufacturing. However, the potential of 3D UV printing of polymeric ionic liquids with metallic fillers for electronic applications remains somewhat limited. In this work, we formulated photocurable resins using a methacrylate-based ionic liquid monomer and a crosslinker, with and without gold nanoparticles as fillers. Our results show that centimeter-scale structures, both free-standing and bonded to a substrate, can be prepared straightforwardly from the formulations using commercial 3D UV printers. The printed structures exhibited high fidelity, a high degree of polymerization, and high thermal stability, with stiffness ranging from 0.2 GPa to 0.5 GPa. Increasing the content of gold nanoparticles in the ionic liquid composites increased the glass transition temperature from −23 °C to −3.5 °C. Polymers without gold nanoparticles had a conductivity of 10^{-6} S cm^{-1}, which increased to 10^{-4} S cm^{-1} in prints with 1 wt% of gold nanoparticles. 3D-printed resistors made from 1 wt% of gold nanoparticles maintained a stable current profile for several hours. Such a result highlights the potential to prepare ionic-liquid-based flexible electronic components using commercial 3D UV printers.

Introduction

Stereolithography (SLA)-3D-printed structures with polymerized or polymeric ionic liquids (PILs) can open new applications.[1–3] Like their parent ionic liquids, millions of synthetically feasible PILs can be developed for specific end uses.[4] Properties like the ion conductivity of PILs[5] can be harnessed, in principle, to prepare flexible 3D UV printed ionotronic devices.[6] Despite a large body of work,[2–4,7] photocurable formulations in which both monomers and crosslinkers are ionic liquids, easy to adapt and compatible with commercial 3D UV-printing are relatively unknown. Crosslinkers derived from ionic liquids can increase the ion density of the resulting PILs, but are rarely reported. The addition of metal fillers to this ionic polymeric matrix can alter properties such as electrical conductivity of the resultant polymer composite. For example, gold nanoparticles (Au-NPs) as a metal filler have been shown to improve the electrical conductivity of the resulting composites.[8–14] However, reports of metal-doped 3D-printed PILs and their characteristics are generally limited.[15] In this work, we present a method for synthesizing an ionic-liquid-based monomer and an ionic-liquid-based crosslinker that are compatible with commercial 3D UV printers. The protocols for printing centimeter-sized structures with Au-NPs embedded in the PIL matrix and the electrical, thermal, and mechanical properties of the printed materials are presented. Notably, we find that Au-NPs embedded in 3D UV-printed PILs exhibit enhanced conductivity. Our work provides a pathway for the future development of photocurable ionic-liquid-based materials for potential use in electronics that are processable with commercial 3D UV printers.

Imidazolium-based ionic liquids are a class of non-homogeneous fluids that are entirely made of ions.[16,17] These liquids can be converted into a solid form through the attachment and subsequent propagation through a polymerizable chemical group inserted onto ionic liquid molecules.[18,19] Numerous combinations of imidazolium cations and their associated anions can be chemically modified into polymerizable monomers.[20,21] If such an ionic liquid monomer is photocurable and compatible with 3D UV printing, the formulations can be utilized to build user-defined PIL structures.[22–26] Many challenges intrinsic to 3D UV printing, including but not limited to developing curing protocols, identifying developing solvents, and establishing post-curing methods, also arise in photocurable ionic liquid formulations.[27–29] In many cases,[30–32] derivatives of 1-vinyl-3-alkyl imidazolium with different counter anions are used in formulations for 3D UV printing, but the vinyl group is less photoactive than acrylate or methacrylate.[31] Also, there is a trend in the literature to use

[a]Department of Chemistry, Xavier University of Louisiana, New Orleans, LA 70125, USA. E-mail: sdutta@xula.edu
[b]School of Polymer Science and Engineering, The University of Southern Mississippi, Hattiesburg, MS 39406, USA

non-ionic crosslinkers, such as poly(ethylene glycol) dimethacrylate, in formulations.[33,34] It should be noted that mixing components in photocurable resins with different polarities can cause inhomogeneity in 3D-printed structures, which can lead to phase segregation over the long term.[35,36] Also, for prototyping, it is necessary to minimize the amount of the starting resin, as ionic liquids are expensive. An understated limitation of broadening the use of PILs is their compatibility with commercial 3D UV printers, particularly those that use liquid crystal display (LCD) projectors. The incident UV light on the resin of LCD UV printers has low intensity, with an average power per surface area of 2–10 mW cm^{-2}. Photocurable ionic liquid resins that yield printed structures capable of addressing the above challenges are required for material adoption.

If the application of 3D UV-printed PIL structures is directed towards electronics, it is necessary to harness the intrinsic ionic conductivity of PILs.[37–40] However, the electrical conductivity of PILs is 100 times lower than that of their parent ionic liquids[5] (typically in the range of 10^{-5} S cm^{-1} or lower) and lower than other electrically conductive polymers[41–43] such as poly(3,4-ethylene dioxythiophene):poly(styrenesulfonate) (PEDOT:PSS).[44] This limitation can be overcome through the addition of a secondary component capable of enhancing the electrical conductivity. Researchers have previously added ionic liquids to the PIL matrix,[45–47] as well as perovskite nanocrystals (PS-NCs), polyoxometalates (POMs), or carbon-based materials to photocurable ionic liquid formulations[48–51] to improve the electrical conductance of PIL composites. However, many of these hybrid systems have not been examined within the framework of SLA technology.[6]

Sevilia *et al.*[52] demonstrated that formulations in which both the monomer and the crosslinker are ionic liquids exhibit improved electrical conductivity. Au NP–ionic liquid-derived polymer composites were earlier shown to enhance electrical conductivity.[53–55] Our novel strategy, therefore, combines three previously proven methodologies to enhance electrical conductivity and appropriate UV response to target 3D UV print techniques in PIL systems: (1) synthesis of ionic liquid monomers based on highly photoreactive methacrylate chemistry, so that they are compatible with commercial 3D UV printers, (2) utilization of a methacrylate-based ionic liquid crosslinker to increase ion density in the cured network, and (3) the addition of a metal dopant, in this case, Au-NPs, to alter the properties of PILs, particularly their electrical conductivities. The overarching strategy of preparing photocurable formulations composed entirely of ionic liquid components will eliminate inhomogeneity associated with mixing components of different polarities.

Monomers of imidazolium-based ionic liquids where the methacrylate group is stationed on the cation are extensively described in the literature.[21,33,56–58] Recently, 3D UV-printed PILs of imidazolium-based ionic liquids with polymerizable anions bearing a methacrylate group have been reported, but they showed poor conductivity.[59] Simulations on PILs based on imidazolium-based ionic liquids, where the cation is polymerized, have been extensively studied and show that conduc-
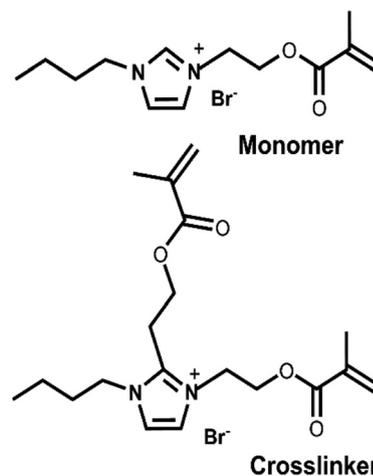

Fig. 1 Photopolymerizable ionic liquid polymer (top) 1-(2-methacryloyloxy)ethyl-3-butylimidazolium bromide and crosslinker (bottom) 3-butyl-1,2-bis(2-(methacryloyloxy)ethyl-3-ethylimidazolium bromide synthesized in this study.

tivity is higher when associated with smaller counterions.[7,38,60] Imidazolium-based PIL matrices prepared from formulations entirely of ionic liquid components, in which the imidazolium cation is methacrylate-functionalized and paired with a small counterion, and which are compatible with 3D UV printing, are missing from the literature. To realize our goals, we synthesized a monofunctional photopolymerizable ionic liquid monomer, 1-(2-methacryloyloxy)ethyl-3-butylimidazolium bromide, and a photopolymerizable ionic liquid crosslinker, 3-butyl-1,2-bis(2-(methacryloyloxy)ethyl)-3-ethylimidazolium bromide, to prepare photocurable ionic liquid formulations (Fig. 1). Au-NPs (15 nm diameter) were added to our formulations to enhance their conductivities. The results demonstrate that PILs without Au-NPs and PILs with Au-NPs can be readily 3D-printed with commercial 3D UV printers. The inclusion of Au-NPs improved electrical conductivity by many orders of magnitude in the PIL networks. PILs, sculpted into resistor-like shapes using 3D printers and inserted into a circuit, sustained a steady electrical current for several hours. The result suggests that PILs can be used to fabricate functional electronic elements by 3D UV printing.

Experimental

Materials

Commercially available 2-bromoethyl methacrylate (95%, Ambeed Inc.), 1-butylimidazole (99%, BeanTown Chemical Inc.), ethyl ether (99%, TCI Ltd), and methylene chloride (99%, TCI Ltd) were used without further purification. Butylated hydroxytoluene (BHT) and pentaerythritol tetraacrylate were obtained from Fisher Scientific. Nuclear magnetic resonance (NMR) spectroscopy and High-Performance Liquid Chromatography (HPLC)/Electrospray Ionization Tandem Mass Spectrometry (ESI-MS) were conducted using a Bruker

AvanceCore 400 MHz NMR spectrometer and a Thermo Scientific™ TSQ Quantis™ Triple Quadrupole mass spectrometer. A Vernier UV-VIS Spectrophotometer was used to obtain the absorbance spectra of the samples.

Synthesis of 1-(2-methacryloyloxy)ethyl-3-butylimidazolium bromide

The procedure used for the synthesis was adopted from a previous report with modification (Scheme 1, top).[58] Briefly, in a 50 mL round-bottom flask, 3.000 g (0.015 mol) of 2-bromoethyl methacrylate was mixed with 1.9298 g (0.015 mol) of 1-butyl imidazole. As both starting materials are liquids, no solvent was required. 0.050 g of BHT was added to the reaction mixture to prevent undesired polymerization. The reaction mixture was stirred at 60 °C for 24 h in the dark. After 24 h, the mixture transformed to a pale, straw-colored viscous liquid. 8 mL of methylene chloride was added to this viscous liquid. The mixture was then transferred to a separatory funnel, where 10 mL of diethyl ether was added, resulting in a two-layer system. The bottom layer (product) was collected. This isolated product was again transferred to a separatory funnel, where 10 mL of fresh diethyl ether was added. The bottom layer was again collected and dried under a high vacuum for several days to obtain the ionic liquid monomer. Characterization of this ionic liquid monomer is given in the SI, S1.

Synthesis of 3-butyl-1,2-bis(2-(methacryloyloxy)ethyl)-3-ethylimidazolium bromide

The ionic liquid crosslinker was synthesized by mixing 2.000 g (0.006 mol) of the above ionic liquid monomer, 1-(2-methacryloyloxy)ethyl-3-butylimidazolium bromide, with an excess of 2-bromoethyl methacrylate (3.318 g, 0.017 mol) in a 50 mL round-bottom flask. As both starting materials are liquids, no solvent was required. A trace amount of BHT (0.080 g) was added to the mixture. This homogeneous mixture was heated at 80 °C for 24 h in the dark with constant stirring. After 24 h, the reaction mixture became a yellowish, viscous solution. Methylene chloride (15 mL) was added to dilute the solution. The solution was then mixed with diethyl ether (15 mL) in a

separatory funnel, which resulted in a two-layer system. The bottom layer (product) was collected. The product was again mixed with 15 mL of diethyl ether in the separatory funnel. The bottom layer was collected and vacuum-evaporated to yield the crosslinker. Characterization of this ionic liquid crosslinker is given in the SI, S2.

Formulation of resin

80 wt% (80 mg) of the monomer was mixed with 20 wt% (20 mg) of the crosslinker in 5 μL of ethanol in a 500 μL Eppendorf tube. To this mixture, ~1 mg of the photoinitiator, diphenyl(2,4,6-trimethylbenzoyl)phosphine oxide (TPO), was added. Several such replicate mixtures in 500 μL Eppendorf tubes were prepared and mounted on a Fisherbrand™ vortex mixer with a tube holder. The blend in 500 μL Eppendorf tubes was shaken in a vortex mixer for 1 hour in the dark to obtain a homogeneous photocurable resin. The resin from these separate 500 μL Eppendorf tubes was combined to prepare a masterbatch. Though we immediately printed with the new masterbatch of the resin, it was not always necessary. The straw-yellow-colored blend remained stable for many days in the dark.

To prepare Au NP-embedded resins, the same procedure as above was followed except that the resin was loaded with an appropriate amount of 15 nm diameter, spherical, dried Au NPs (NanoComposix Inc.). As before, the mixture was shaken in 500 μL Eppendorf tubes for at least 1 hour using a vortex mixer to obtain pale-blue resins, which were then combined for printing.

3D printing protocols

A commercial 3D LCD UV printer (405 nm, Halot Sky, Shenzhen Creality 3D Technology Co., Ltd) with an intensity of 4 mW cm^{-2} was used for our studies. User-defined structures were created using the Tinkercad 3D modeling program and then converted with Halot Box slicer (Shenzhen Creality 3D Technology Co., Ltd) software to a format compatible with 3D printing. The printing was done directly on the built glass plate on the instrument without the resin vat. The printing substrate was either glass microscope coverslips (Fisher
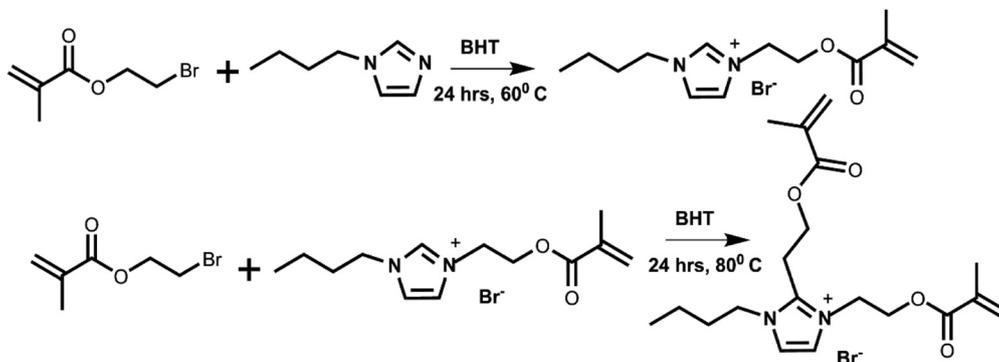
Scheme 1 Synthesis of the monomer (top) and the crosslinker (bottom). Butylated hydroxytoluene (BHT) acts as an inhibitor.
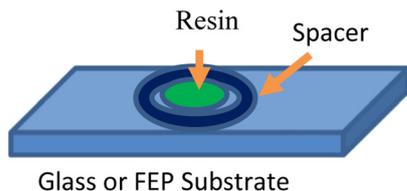
Fig. 2 (Top) Schematic of the assembly for preparing printed structures.

Scientific Inc., thickness: 0.13–0.17 mm) or a square piece (4 in × 4 in) of fluorinated ethylene propylene (FEP) (Club 3D, thickness: 0.1 mm). Teflon O-rings or single-well SecureSeal™ imaging spacers (Grace Bio-Labs Inc.) were used as micro-reservoirs (vat) within which centimeter-scale structures were printed. SecureSeal™ imaging spacers have adhesive that bonds to the glass, preventing leakage of the resin. Teflon O-rings require a weight to hold them in position. Spacers in FEP substrates required weights to hold them in position. The reservoirs (vat) could hold 1–2 mL of resin (Fig. 2).

To print, the substrate was first carefully aligned on the glass build plate, so that the UV projection of the printer was at the center of the O-ring/SecureSeal™ created a reservoir. Next, the file with the desired shape was run on the printer software. A typical printing run was ~2–5 minutes, depending on the complexity of the structure. The developed structure was washed with ethanol at least three times to remove the uncured resins. The structure was then post-cured in a UV oven (Analytik Jena, AG) for 30 min to ensure full conversion of the print. Structures printed onto FEP were easily removed from the substrate surface. More details on the printing work-flow and fidelity assessment in the *X*- and *Y*-directions are provided in the SI, S3. Printed examples are given in the SI, S4. Though the Halot Sky model was used in the majority of this work, we tested our formulations with another commercial 3D LCD UV printer (Photon Mono 4, Shenzhen Anycubic Technology Co., Ltd) with similar results (SI, S5).

Infrared spectroscopy

Infrared measurements were performed with an FTIR (Nexus 670 Avatar Nicolet, Thermo Scientific Inc., or ALPHA II, Bruker Co.) equipped with an attenuated total reflectance (ATR) accessory. In a typical run, 3D prints were pressed on the ATR diamond crystal. 16 scans in the region between 4000 and 500 cm^{-1} were carried out for each sample with a resolution of either 2 cm^{-1} or 4 cm^{-1}. The results were analyzed in OMNIC (Thermo Scientific Inc.), in OPUS (Bruker Co.) or in Igor Pro software (WaveMetrics Inc.).

Scanning electron microscopy (SEM)

PIL samples were measured with a Hitachi Tabletop micro-scope (Flex 1000 II). The equipment was connected to an Energy Dispersive Spectroscopy (EDS) system (Oxford Instruments). The samples were placed on a silicon wafer coated with gold, which was attached to an aluminum holder

with double-sided carbon conductive tape before being intro-duced into the SEM chamber. As structures printed on glass substrates were bonded to it, small pieces of the structures were cut and placed on the silicon wafer for SEM observation. On the other hand, structures made on FEP substrates could be peeled and placed on the silicon wafer for SEM observation. The samples did not require sputter coating as PILs are con-ductive materials. SEM images were analyzed using Hitachi software, whereas EDX was captured using Oxford Instruments Aztec software.

Electrical conductivity

To measure the electrical conductivity, discs ranging from 10 mm to 15 mm in diameter and 0.5 mm to 0.2 mm in thick-ness were printed with the formulations as described above. The electrical conductivity of these discs was measured using an Ossila four-point probe station with soft probe tips. At least three discs were prepared from a chosen formulation for con-ductivity measurements. Each disc was tested in three different sample areas.

Thermal gravimetric analysis with mass spectroscopy (TGA-MS)

Mass loss and gas evolution were measured under nitrogen using a TA Instruments Discovery Series TGA-MS equipped with a 300 amu quadrupole mass spectrometer. Samples with a mass of 1.8 mg ± 1.0 mg were heated under a nitrogen purge to 800 °C at 10 °C min^{-1}. The full 1–300 amu range was scanned at a rate equal to 3 scans per min for the full duration of the heating process.

Differential scanning calorimetry (DSC)

DSC was performed using a TA Instruments Discovery 2500 in a nitrogen atmosphere (50 mL min^{-1}). Samples with a mass of 5.3 mg ± 0.5 mg were loaded into hermetically sealed alumi-num pans and heated from −80 °C to 50 °C at 10 °C min^{-1} and cooled to −80 °C at 10 °C min^{-1} before reheating to 50 °C at 10 °C min^{-1}. The glass transition temperature was deter-mined between −40 °C and 40 °C for most systems using the midpoint half-height method, representing the halfway point of the vertical baseline shift.

Mechanical analysis

Nanoindentation experiments were performed using a KLA iNano with an InForce 50 actuator and a Berkovich indenter. Samples were indented using continuous stiffness measure-ment to a target depth of 2000 nm with a surface approach vel-ocity of 50 nm s^{-1} at a surface distance of 2500 nm. The values of Young's modulus (E) for each sample were calculated using the Oliver–Pharr method using the equation

$$E = (1 - \nu^2) \left[\frac{1}{E_r} - \frac{(1 - \nu_i^2)}{E_i} \right]^{-1}$$

where ν is the Poisson's ratio of the sample, ν_i is the Poisson's ratio of the indenter, E_r is the reduced Young's modulus and

E_i is the modulus of the indenter. At least three different points from three different samples were measured, and their average was reported in this work.

Results and discussion

The monosubstituted methacrylate-labeled imidazolium-based ionic liquid from 2-bromoethyl methacrylate is well known in the literature[56–58,61] and yields the monomer 1-(2-methacryloyloxy)ethyl-3-ethylimidazolium bromide (Fig. 1 (top)). We found that the inhibitor BHT is essential in the reaction scheme to prevent unwanted polymerization. Characterization studies of the synthesized monomer using NMR, MS, and IR are consistent with earlier reports (see the SI, S1).[56–58,61] However, synthesizing the crosslinker as proposed in Scheme 1 (bottom) was challenging. Our scheme assumed that performing the reaction at a higher temperature (80 °C) favored selective substitution at the C2-position of the monomer,[62,63] 1-(2-methacryloyloxy)ethyl-3-ethylimidazolium bromide, resulting in two methacrylate groups in the imidazolium ring. In our HPLC/ESI-MS measurements in positive ion mode (SI, S2), we observe three m/z peaks at 113.11, 237.15, and 351.13. The first peak corresponds to the ethyl methacrylate ion, which may originate from the fragmentation at the C2-position of the cation from the proposed crosslinker structure (Fig. 1 (bottom)) or the fragmentation of unconverted 2-bromoethyl methacrylate during the acquisition process. The dominating ESI-MS peak of m/z 237.15 represents the $[M]^+$ of the monomer 1-(2-methacryloyloxy) ethyl-3-ethylimidazolium bromide. The intensity of the peak suggests that most of the monomer did not convert to the proposed crosslinker structure during the synthesis process. In other words, the majority of the product in our preparation method for the crosslinker is the ionic liquid monomer. The peak at m/z 351.13 indicates that a second ethyl methacrylate is attached to the monomer, although the structure remains unclear. The NMR of the crosslinker is complex, where we see peaks that hint at the presence of both the monomer and the crosslinker, but cannot be clearly assigned. IR data do not clarify the characterization when compared to the monomer. From NMR and ESI-MS characterization, we hypothesize that our synthesis method generates a dilute solution of ionic liquid crosslinker(s) (<5%) in the ionic liquid monomer. Our described method of preparing the dilute crosslinker solution is straightforward but, most importantly, reproducible (*vide infra*). We refer to this dilute ionic liquid crosslinker solution in the ionic liquid monomer as the crosslinker in the rest of the text. It should be noted that no polymerized structures were observed from the synthesized ionic liquid monomer without the crosslinker or formulations of the ionic liquid monomer with 2-bromoethyl methacrylate without the crosslinker.

Out of many possible combinations of ionic liquid monomer and crosslinker formulations, we selected 80 wt% of the synthesized ionic liquid monomer and 20% of the crosslinker monomer mixture dissolved in minimal ethanol, referred to henceforth as 80/20 ionic liquid photocurable formulation, as the photocurable resin for the studies. PILs made from this resin are denoted as 80/20 polymer in the figures. Formulations with crosslinker contents below 20 wt% resulted in structures whose integrity was compromised during the rinsing process after printing. A possible explanation for the need for a high crosslinker concentration (20 wt%) in the resin is that the crosslinker, as explained above, is mainly a solution of starting synthesized ionic liquid monomers, with a small percentage of the actual crosslinker. Increasing the amount of crosslinker resin possibly increases the concentration of the actual crosslinker. To obtain gold nanoparticle (Au-NPs, 15 nm diameter)-embedded PIL composites, resins were prepared by dispersing the Au-NPs *via* agitation in the above 80/20 ionic liquid photocurable formulation. In this work, we tested 1 wt% of Au-NPs or 2 wt% of Au-NPs in an 80/20 ionic liquid photocurable formulation for 3D UV-printed PIL composites. In all the formulations, ethanol was used as a diluent to facilitate the solubility of the photoinitiator, TPO. Unlike commercial 3D UV printers, which require at least 50 mL of resin to fill the vat or tank, this work used a spacer as a vat (Fig. 2), which only needed ~1–2 mL of the prepared resin for 3D printing, vastly reducing the amount of material and the cost required for prototyping with ionic liquids. A drawback was that we were limited to centimeter-scale structures. We note that isopropanol, which is commonly used for washing uncured resins, distorted the printed structures.[64] We found 70% w/v ethanol to be the best developing solvent for our prints. An advantage of ethanol as the developing solvent was that we could reuse uncured materials by rotovaping the solvent, thereby minimizing waste. All printed structures were cured in a UV oven after washing. We note that post-curing can also be achieved by heating the 3D prints to 100 °C, but this process often results in bubbles within the matrix. We assume that any uncured resin trapped in the matrix is cured in the post-curing process. A selection of printed products is shown in Fig. 3. More examples of printed products are given in the SI, S4. The printed products exhibited high fidelity in the X and Y directions (see the SI, S3). The height (Z-axis, thickness) of the structures depended on the spacer and the amount of liquid. Typically, the height of the printed structures varied from 0.2 mm to 0.5 mm. The 3D-printed structures were pale brown, soft, and stretchable for the 80/20 ionic liquid photocurable formulation and deep purple for Au-NP-filled PIL composites. Printed structures firmly adhered to glass substrates but could be peeled off of FEP substrates to obtain freestanding structures. Overall, our results indicate that the 80/20 ionic-liquid photocurable formulation and its Au-NP-filled resins are promising candidates for printing centimeter-scale PIL objects with commercial 3D UV printers, using both glass and FEP as substrates.

SEM images (Fig. 4) provide insights into the morphology of the 3D prints. The structures of the 80/20 polymer were smooth. EDS analysis clearly showed the presence of bromide (the anion in the photocurable ionic liquids) in the X-ray emission spectrum. SEM images of 1 wt% of Au-NPs in the 80/20
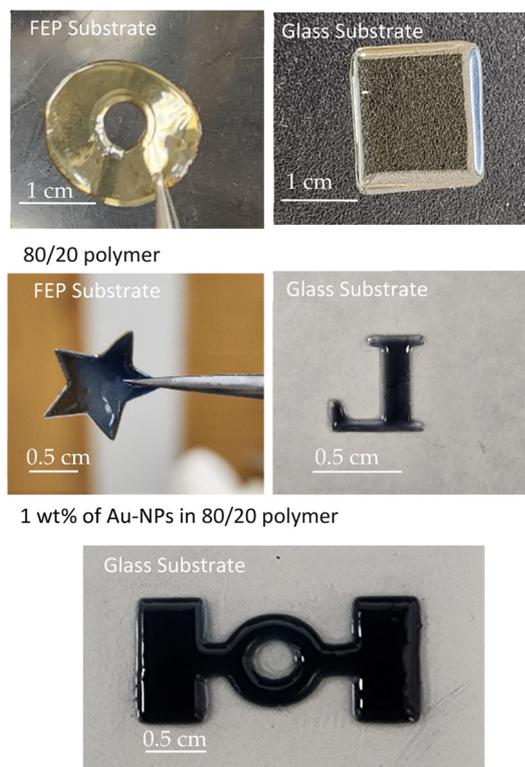
Fig. 3 Collection of 3D UV-printed structures with different formulations. Prints from FEP substrates were free-standing. Optical scales are approximate.

ionic liquid photocurable formulation showed a smooth surface. However, there were also scattered spots of aggregation on the surface. Such clusters, assumed to be Au-NPs, are

more prominent in 2 wt% of Au-NPs in the 80/20 mixture (see the SI, S6). UV-Vis analysis supports the presence of Au-NP clusters within the matrix. Our Au-NPs, when dispersed in ethanol, have a single strong UV absorption peak at ~520 nm due to localized surface plasmon resonance absorption, but when the Au-NPs are embedded in the PIL samples, we find the UV absorption, as seen in Fig. 4, to be red-shifted, broad, and weak (Fig. 4, bottom, right). Such changes are indicative of the agglomeration of NPs, which is not uncommon in Au NPs embedded in a polymer matrix.[65,66]

The degree of polymerization is an important characteristic that influences material properties. Typically, the degree of polymerization for methacrylate-based resins is determined by infrared spectroscopy by comparing the intensity of the infrared absorption peak at 1637 cm^{-1} [ν(C=C)] of the unreacted methacrylate groups to the intensity of infrared absorption of different internal standard peaks. However, there are discrepancies in such assessments requiring baseline correction due to absorption artifacts in polymers.[67] This study found such artifacts detrimental in our PIL analysis due to featureless background absorption in the 1637 cm^{-1} region. An alternative, which works for our studies, suggested by Delgado et al.,[68] is assessing the signal intensity of the C–O stretch doublet of the methacrylate group approximately at 1300 cm^{-1} and 1320 cm^{-1}.

The doublet peaks shift to lower wavenumbers upon polymerization. It is clear from Fig. 5, which shows barely any residual signal from the doublet peak, that the polymerization is at or near full conversion. We observe the same high degree of polymerization in all our Au NP-embedded PILs. Example infrared spectra of the other 3D-printed samples are provided in the SI, S8. As our experiments are conducted under ambient conditions, we expect water to be present in the matrix.
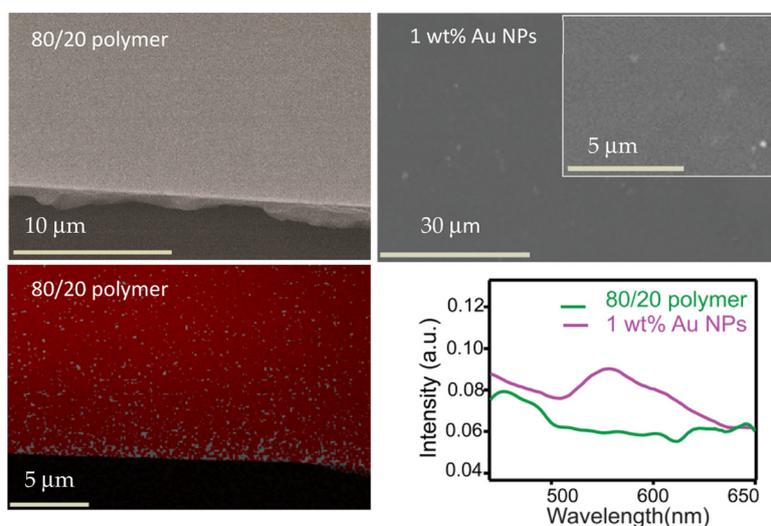

Fig. 4 (Left) SEM image of a printed structure with an EDS map of bromine (red) of a printed area with an 80/20 polymer. (Right) SEM image of a printed structure with an 80/20 polymer with 1 wt% of Au-NPs. The inset in the SEM image shows hints of agglomeration. (Bottom, right) UV-Vis spectrum of the 80/20 polymer, which is featureless between 550 nm and 650 nm but shows a broad weak peak at ~570 nm when Au-NPs are present.
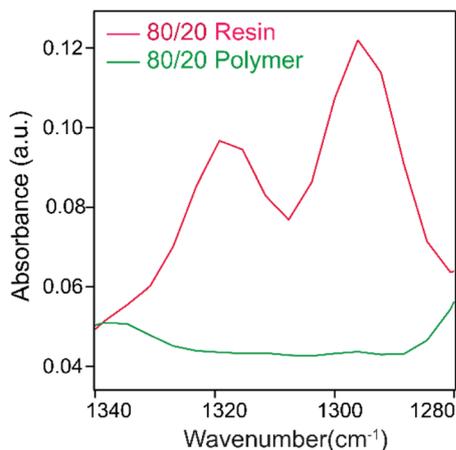
Fig. 5 ATR-FTIR spectrum (red) of the monomer of the 80/20 ionic liquid photocurable formulation, showing a characteristic C−O stretch doublet at 1300 cm^{-1} and 1320 cm^{-1} of the methacrylate monomer. Upon polymerization, the infrared signatures of the doublets shift to lower wavenumbers. As the spectrum (black) does not show residual absorption in the C−O stretching region after photopolymerization, we conclude that there is a high degree of polymerization.

Indeed, we observe a broad absorption band at ∼3400 cm^{-1}, which is typical of the OH stretching vibration of water in all our PILs. Broadly, the results indicate that our 3D UV printing protocols can achieve a high degree of polymerization with the resins.

Fig. 6 shows the TGA results of PILs prepared from the 80/20 photocurable formulation and those with 1 wt% and 2 wt% Au NP-embedded in the PIL matrix from 90 °C to 800 °C under a nitrogen atmosphere. The PILs were compared with a control, which was printed from 80 wt% of the synthesized ionic liquid monomer and 20 wt% of a commercial non-ionic crosslinker monomer, pentaerythritol tetramethacrylate. We observe that, like parent ionic liquids and other reported PILs,[69,70] all our PILs exhibited high thermal stability. As seen in Fig. 6 (top), the PILs had an initial loss (∼10% of weight) upon heating until ∼250 °C, possibly due to loss of humidity (water) in the matrix. Above 250 °C, a rapid onset of mass loss is observed in all cases, indicating depolymerization of the methacrylate group or other widespread degradation events.[71,72] However, it is evident from Fig. 6 (top) that the degradation pattern of the control PIL differs from others after ∼250 °C. One reason for the difference may be the low actual crosslinker concentration (<5%) in the PIL matrices. We also observe that, unlike the control, PILs with an ionic liquid crosslinker exhibit two additional degradation events at ∼350 °C and ∼450 °C. The difference may be due to the nature of the water in the matrices. Recall that we have observed evidence of water in all our PILs *via* infrared spectroscopy. TGA-MS provides insights into the nature of this water in PIL matrices. Analyzing the ion current for *m/z* 18 amu, as presented in Fig. 6 (bottom), shows only one peak for the control, whereas all others exhibit two peaks. The observation implies that matrices prepared using our synthesized ionic-liquid
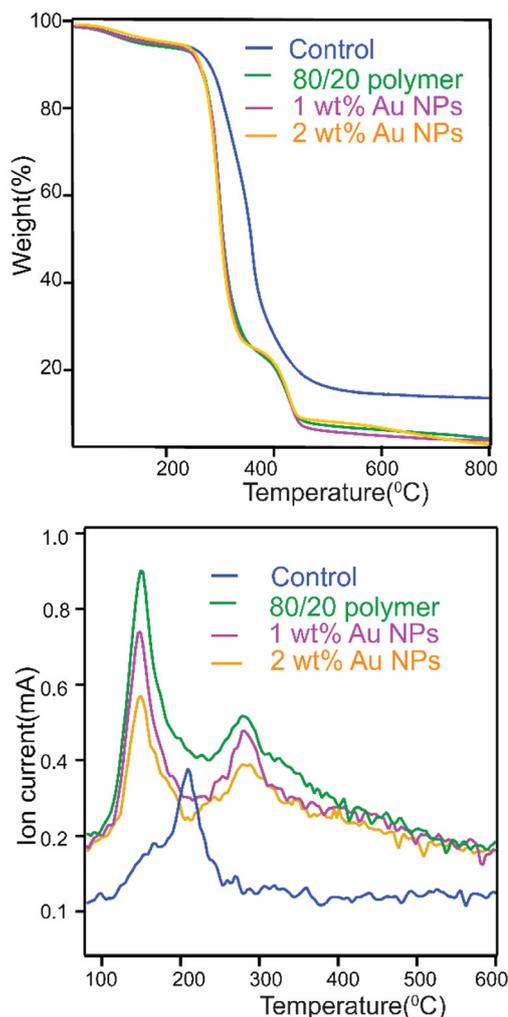

Fig. 6 (Top) TGA shows that the polymers are stable at least to 200 °C. (Bottom) TGA-MS scanned at *m/z* 18 amu. The control is a PIL with the commercial non-ionic crosslinker pentaerythritol tetramethacrylate.

crosslinker contain two distinct types of bound water: tightly bound and loosely bound. The water that evolves in our TGA-MS experiment at ∼300 °C may indicate tightly bound water molecules in the matrices, possibly due to hydrogen bonding between bromide anions and water molecules. The presence of tightly bound water molecules may be one reason why the thermal degradation patterns of printed polymers using the ionic liquid crosslinker, with or without Au-NPs, differ from those of the control. We note that TG-MS also indicates that our matrices are free of solvents or starting monomers. In short, our PILs are thermally stable, where the presence of the ionic liquid crosslinker changes how the polymers degrade when compared to the commercial non-ionic liquid crosslinker.

The glass transition temperature (T_g) of all the polymers, determined by DSC, was below room temperature (SI, S9). Thus, it is not surprising that our polymers were soft and flexible in the printed state. The PIL obtained from the 80/20

photocurable formulation had a T_g of −23 °C, whereas PILs obtained from 80/20 photocurable formulations of 1 wt% of Au-NPs and 2 wt% of Au-NPs had T_g values of −7.2 °C and −3.5 °C, respectively. An increase in the T_g of Au-NP-embedded PIL composites is possibly due to the restriction of polymer chain mobility due to the presence of nanoparticles.[73]

The stiffness of the printed materials was assessed using nanoindentation and the results are presented in Fig. 7. Control PILs prepared from 80 wt% of the ionic liquid monomer and 20 wt% of a commercial non-ionic crosslinker monomer, pentaerythritol tetramethacrylate, had the highest modulus of ~3.2 GPa. It is an order of magnitude higher than that of polymers printed with our 80/20 ionic liquid photocurable formulation (0.46 ± 0.04 GPa). One explanation for this observation is that the commercial crosslinker has four methacrylate groups, whereas our synthesized ionic liquid-based crosslinker contains only two photocurable groups. The large difference may also arise from a lower effective crosslink density in the PILs than in the control. Although both PILs and the control were prepared using 20 wt% of the crosslinker in the formulation, in reality, the ionic liquid crosslinker is a dilute solution (<5%) of the actual crosslinker(s) in the ionic liquid monomer. The presence of tightly bound water, as observed in our TGA-MS experiments on PILs, may also contribute to the observed trends in tensile strength. Water absorbed into a polymer matrix can act as a plasticizer, disrupting intermolecular forces between polymer chains. Such disruption can significantly reduce tensile strength. Apart from the difference between PILs and the control, there are differences among PILs. The Young's modulus of structures with 1 wt% of Au NPs in an 80/20 ionic liquid photocurable formulation was 0.34 ± 0.04 GPa, slightly higher than its 2% counterpart, which was 0.28 ± 0.03 GPa. We assume that increased agglomeration with higher Au-NP concentrations

creates localized weak points in the composite, thereby reducing the tensile strength.

To test the potential application in electronics, we measured the conductivity of printed circular PIL films (thickness ~0.5 mm) using a four-point probe method. Our instrument uses a direct current voltage and measures the current across the sample to calculate conductivity. It is relevant to electronics for initial assessment, as most electronic devices operate on direct current. Again, as a control, we used 80 wt% of the ionic liquid monomer and 20 wt% of a commercial non-ionic crosslinker monomer, pentaerythritol tetramethacrylate. The conductivity of the control films was below the detectability limit of our four-point probe instrument. In other words, no conductivity was detected for printed films with our control formulation. On the other hand, printed films of the 80/20 ionic liquid photocurable formulation consistently exhibited a conductivity of approximately 10^{-6} S cm^{-1} (Fig. 8, 80/20 polymer). The measured conductivity is consistent with other reports.[38] It supports our earlier assumption that an ionic liquid-based crosslinker in PIL matrices increases ion densities, enabling improved conductivity. However, it is pertinent to note that our crosslinker is a dilute solution in the monomer, as mentioned earlier, which may result in lower-than-expected ion densities in the cured networks, reducing ion conductivity. Upon introducing Au-NPs into the ionic liquid resins, the conductivity of the printed PIL further increased from 10^{-6} S cm^{-1} to 10^{-4} S cm^{-1}. The two-order-of-magnitude increase in conductivity may be attributable to additional electronic pathways and the high surface area of the Au nanoparticles, in addition to the intrinsic ion-transport mechanism within PILs.[54,55] However, the exact mechanism of enhancement requires further investigation with tools such as electrochemical impedance spectroscopy to determine the con-
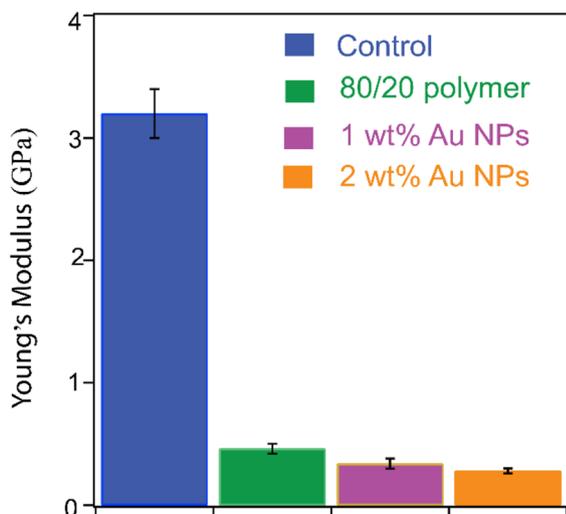

Fig. 7 Modulus of PILs measured by nanoindentation. The control is a PIL with the commercial non-ionic crosslinker pentaerythritol tetramethacrylate.
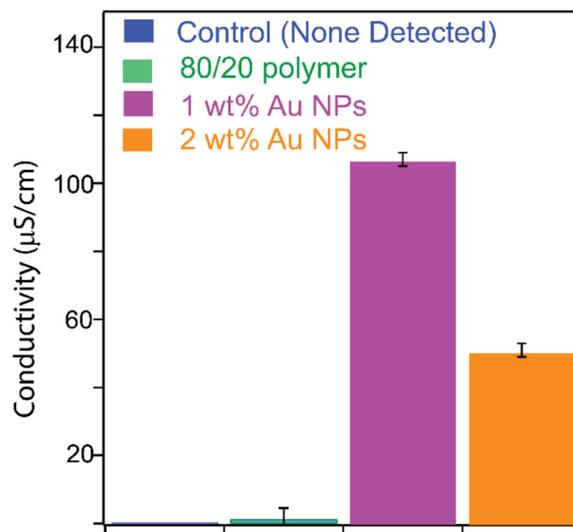

Fig. 8 Conductivity of PILs measured using a four-point station. The control is a PIL with the commercial non-ionic crosslinker pentaerythritol tetramethacrylate.

tributions of electronic and ionic processes in the system.[53,74] It is also possible that bound water, which we observed in thermal studies and infrared spectra, may play a role in conduction, which requires further study. Regardless of the mechanism, materials with conductivity in the range of 10^{-4} S cm^{-1} are attractive for use in flexible electronics. The trend shown in Fig. 8 indicates a trade-off between increased Au-NP concentration and observed conductivity in the resin, consistent with observations reported elsewhere, in which the aggregation of NPs at higher concentrations is suggested to result in poor bulk properties of polymer–nanoparticle composites.[75,76] Overall, our studies show that structures prepared from 1 wt% of Au-NPs in the 80/20 ionic liquid photocurable formulation were best in terms of both printing and conductivity.

In order to validate whether 1 wt% of Au-NPs in the 80/20 photocurable formulation can be used as the construction material for a functional element in a circuit, we designed and 3D-printed a centimeter-scale structure in the shape of a resistor (~1 cm (l) × 1 cm (w) × 200 mm (h)) with a connector pad (~0.2 cm (l) × 0.2 cm (w) × 500 μm (h)) on a microscope glass slide using the same method as described earlier. The design serves as a proof of concept, showing that functional elements can be built using our ionic liquid formulation. Fig. 9 (top, left) is a representative of one such device. The same design on FEP substrates to obtain free-standing 3D-printed resistors was found to be mechanically weak, so our studies were con-

fined to resistors printed on glass substrates. In our scheme, as shown in the circuit diagram in Fig. 9 (bottom left), the printed resistor was incorporated into an electrical circuit and tested under ambient conditions (see the SI, S10, for more details). Current flowing through the circuit was used as the metric for assessing the functionality of the printed resistor. Our results were qualitative but indicated that applying a 30 V direct current power supply produced a detectable current in the microampere range through the circuit. Fig. 9 (top, right) shows current responses from a circuit, with a printed resistor, undergoing turn-on and turn-off cycles separated by a 24-hour gap. Turning off the circuit with the printed resistor for 24 hours and restarting it again for 2 hours showed that the current was within 5% of the original value. Encouraged by the results, we independently printed and tested eight additional resistors using the design described above. The measured currents were between 23 mA and 18 mA from the printed resistors (Fig. 9 (bottom, right)). The current in each circuit remained stable for two hours of continuous operation, with minimal deviation from the mean. Using the measured current as a quality control metric, the coefficient of variability was about 5.8% among devices. Given that the devices were made from different batches of starting materials, the low coefficient of variability not only demonstrates reproducibility but also suggests batch-to-batch consistency and the robustness of our printing protocols. One limitation observed was
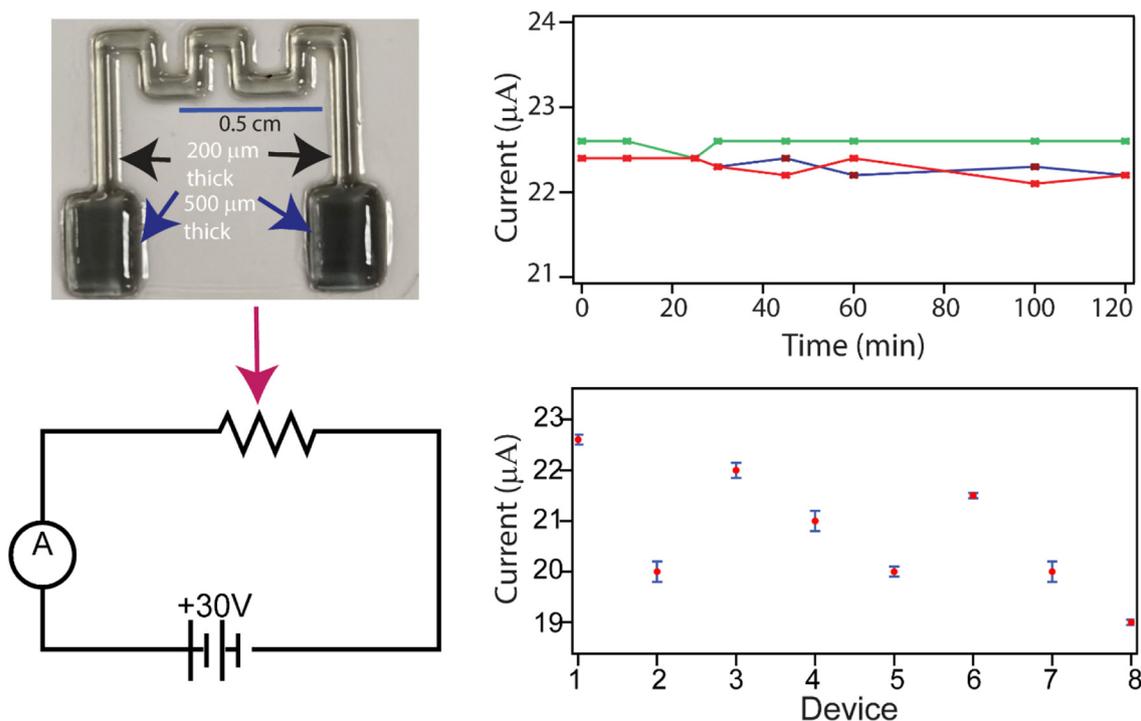

Fig. 9 A printed resistor (top, left) with 1 wt% of Au NPs in the 80/20 polymer on a glass substrate, when inserted in the circuit (bottom, left), showing the flow of current in the microampere range when 30 V is applied. The current profile of a printed resistor (top, right) running for two hours with on-and-off cycles with a 24-hour gap is represented with green, blue, and red lines. The profile of average current flowing (bottom, right) through printed resistors (8 different resistors and 8 devices) for two hours. Note that the deviation (blue bars) of current from the average value (red dot) is small, indicating that each device is robust within the experimental timescale.

that the continuous operation of the circuit for more than 5 hours resulted in a 20% loss of the magnitude of the current flowing through the circuit. This may be due to heating effects that may have resulted in polymer degradation. We also observed yellowing[77] of the polymer at the contact points of the resistor with the circuit. This phenomenon was observed irrespective of whether the contact material to the PIL resistor was copper or nichrome wires. Often, wire-to-pad disconnection was the main cause of failure in extended operation. Overall, our results demonstrate that 3D-printed PIL structures are stable against the flow of electrical current for a short duration. We envisage that our concept validation will inspire others to use our formulations to prepare user-defined structures for a specific task (*e.g.*, CO_2 sensing) for integration into a working circuit.

Conclusion

In this manuscript, we present the synthesis of a photocurable methacrylate-based ionic liquid monomer and a crosslinker compatible with commercial 3D UV printing. PILs in which the crosslinker is an ionic liquid are expected to exhibit lower electrical resistance due to an increase in ionic densities as opposed to commercial non-ionic liquid crosslinkers. We incorporated Au-NP PILs to modulate the properties of the 3D prints, including electrical conductivity. Characterization of PILs with or without Au-NPs indicates high thermal stability and a high degree of polymerization, but their tensile strength is <1 GPa. The PIL-printed materials were hygroscopic, with evidence of tightly bound water molecules within the matrices. The protocol for 3D printing was straightforward, resulting in structures with high fidelity using commercial 3D UV printers. Printed polymer matrices with 1 wt% of Au-NPs in 80 wt% of the synthesized ionic liquid monomer and 20 wt% of the ionic liquid crosslinker showed the highest electrical conductivity of $\sim 10^{-4}$ S cm^{-1}. Our proof-of-principle experiment with centimeter-scale resistors fabricated from this formulation demonstrated a stable current for several hours. Such a demonstration provides a template for printing PIL-based sensors for detecting gases, particularly CO_2, as ionic liquids are known to be selective for this gas. For example, the bromide anion in our work can be replaced by the dicyanamide anion, which is known to absorb large amounts of CO_2 and thus can enable the development of PIL-based chemiresistive sensors. Broadly, our work enables testing of many innovative designs, such as modifying the anions of ionic-liquid monomers to control the physicochemical properties of the printed matrices or introducing additives, such as carbon fibers, to improve tensile strength with fast turnaround times. Instead of Au-NPs, other metal NPs, such as copper or nickel, can be added to the PIL matrix. We expect our work to enable the printing of smart polymeric structures[78] by exploiting the tunable properties of ionic liquids with existing commercial additive manufacturing.

Conflicts of interest

There are no conflicts to declare.

Data availability

The data supporting this article have been included as part of the supplementary information (SI). Supplementary information is available. See DOI: https://doi.org/10.1039/d6lp00007j.

Acknowledgements

References

1 M. Criado-Gonzalez, A. Dominguez-Alfaro, N. Lopez-Larrea, N. Alegret and D. Mecerreyes, *ACS Appl. Polym. Mater.*, 2021, **3**, 2865–2883.
2 Q. Li, F. Yan and J. Texter, *Chem. Rev.*, 2024, **124**, 3813–3931.
3 O. Lebedeva, D. Kultin and L. Kustov, *Eur. Polym. J.*, 2024, **203**, 112657.
4 R. Salas, R. Villa, F. Velasco, F. G. Cirujano, S. Nieto, N. Martin, E. Garcia-Verdugo, J. Dupont and P. Lozano, *Green Chem.*, 2025, **27**, 1620–1651.
5 H. Ohno, M. Yoshizawa and W. Ogihara, *Electrochim. Acta*, 2004, **50**, 255–261.
6 H. Yuk, B. Lu, S. Lin, K. Qu, J. Xu, J. Luo and X. Zhao, *Nat. Commun.*, 2020, **11**, 1–8.
7 Y. Cheng, J. Yang, J. H. Hung, T. K. Patra and D. S. Simmons, *Macromolecules*, 2018, **51**, 6630–6644.
8 T. Nezakati, A. Seifalian, A. Tan and A. M. Seifalian, *Chem. Rev.*, 2018, **118**, 6766–6843.
9 M. K. Corbierre, N. S. Cameron, M. Sutton, S. G. J. Mochrie, L. B. Lurio, A. Rühm and R. B. Lennox, *J. Am. Chem. Soc.*, 2001, **123**, 10411–10412.
10 L. Kool, A. Bunschoten, A. H. Velders and V. Saggiomo, *Beilstein J. Nanotechnol.*, 2019, **10**, 442–447.
11 S. Fu, Z. Sun, P. Huang, Y. Li and N. Hu, *Nano Mater. Sci.*, 2019, **1**, 2–30.
12 N. Toshima and N. Jiravanichanun, *J. Electron. Mater.*, 2013, **42**, 1882–1887.
13 D. Mecerreyes, *Prog. Polym. Sci.*, 2011, **36**, 1629–1648.
14 S. Das, M. A. H. Klos, T. Kraus and R. Bennewitz, *Nanoscale*, 2026, **18**, 1643–1650.

15 S. Park, W. Shou, L. Makatura, W. Matusik and K. (Kelvin) Fu, *Matter*, 2022, **5**, 43–76.

16 T. Welton, *Biophys. Rev.*, 2018, **10**, 691–706.

17 J. P. Hallett and T. Welton, *Chem. Rev.*, 2011, **111**, 3508–3576.

18 S. Miralles-Comins, M. Zanatta and V. Sans, *Polymers*, 2022, **14**, 5121.

19 K. R. Hossain, P. Jiang, X. Yao, X. Yang, D. Hu and X. Wang, *J. Ionic Liq.*, 2023, **3**, 100066.

20 A. Bagheri and J. Jin, *ACS Appl. Polym. Mater.*, 2019, **1**, 593–611.

21 M. D. Green and T. E. Long, *Polym. Rev.*, 2009, **49**, 291–314.

22 N. Nishimura and H. Ohno, *Polymer*, 2014, **55**, 3289–3297.

23 R. Guterman and C. A. Smith, *Isr. J. Chem.*, 2019, **59**, 803–812.

24 Z. Wang, J. Zhang, J. Liu, S. Hao, H. Song and J. Zhang, *ACS Appl. Mater. Interfaces*, 2021, **13**, 5614–5624.

25 I. Roppolo, M. Zanatta, G. Colucci, R. Scipione, J. M. Cameron, G. N. Newton, V. Sans and A. Chiappone, *React. Funct. Polym.*, 2024, **202**, 105962.

26 S. Miralles-Comins, M. Zanatta, S. G. Embid, M. Alleva, A. Chiappone, I. Roppolo, S. G. Mitchell and V. Sans, *Device*, 2024, **2**, 100224.

27 H. Quan, T. Zhang, H. Xu, S. Luo, J. Nie and X. Zhu, *Bioact. Mater.*, 2020, **5**, 110–115.

28 S. F. Iftekar, A. Aabid, A. Amir and M. Baig, *Polymers*, 2023, **15**, 2519.

29 A. Jandyal, I. Chaturvedi, I. Wazir, A. Raina and M. I. Ul Haq, *Sustainable Oper. Comput.*, 2022, **3**, 33–42.

30 D. R. Nosov, E. I. Lozinskaya, D. Y. Antonov, D. O. Ponkratov, A. A. Tyutyunov, M. A. Eddine, C. Plesse, D. F. Schmidt and A. S. Shaplov, *ACS Polym. Au*, 2024, **4**, 512–526.

31 K. R. Hossain, P. Jiang, X. Yao, X. Yang, D. Hu and X. Wang, *J. Ionic Liq.*, 2023, **3**, 100066.

32 K. E. O'Harra, G. M. Timmermann, J. E. Bara and K. M. Miller, *ACS Appl. Polym. Mater.*, 2021, **3**, 1995–2004.

33 A. S. Shaplov, P. S. Vlasov, E. I. Lozinskaya, D. O. Ponkratov, I. A. Malyshkina, F. Vidal, O. V. Okatova, G. M. Pavlov, C. Wandre, A. Bhid, M. Schönhof and Y. S. Vygodskii, *Macromolecules*, 2011, **44**, 9792–9803.

34 K. Nakamura and K. Fukao, *Polymer*, 2013, **54**, 3306–3313.

35 V. Bocharova and A. P. Sokolov, *Macromolecules*, 2020, **53**, 4141–4157.

36 *Electrochemical Aspects of Ionic Liquids*, ed. H. Ohno, Wiley, New York, 1st edn, 2005.

37 E. M. Thomas, P. H. Nguyen, S. D. Jones, M. L. Chabinyc and R. A. Segalman, *Annu. Rev. Mater. Res.*, 2021, **51**, 1–20.

38 E. W. Stacy, C. P. Gainaru, M. Gobet, Z. Wojnarowska, V. Bocharova, S. G. Greenbaum and A. P. Sokolov, *Macromolecules*, 2018, **51**, 8637–8645.

39 H. Kokubo, R. Sano, K. Murai, S. Ishii and M. Watanabe, *Eur. Polym. J.*, 2018, **106**, 266–272.

40 B. D. Martin, N. Nikolov, S. K. Pollack, A. Saprigin, R. Shashidhar, F. Zhang and P. A. Heiney, *Synth. Met.*, 2004, **142**, 187–193.

41 S. Sen, S. E. Goodwin, P. V. Barbará, G. A. Rance, D. Wales, J. M. Cameron, V. Sans, M. Mamlouk, K. Scott and D. A. Walsh, *ACS Appl. Polym. Mater.*, 2021, **3**, 200–208.

42 P. S. C. de Oliveira, S. A. Alexandre, G. G. Silva, J. P. C. Trigueiro and R. L. Lavall, *Eur. Polym. J.*, 2018, **108**, 452–460.

43 C. Fu, G. Homann, R. Grissa, D. Rentsch, W. Zhao, T. Gouveia, A. Falgayrat, R. Lin, S. Fantini, C. Battaglia, C. Fu, G. Homann, R. Grissa, D. Rentsch, W. Zhao, C. Battaglia, T. Gouveia, A. Falgayrat, R. Lin and S. Fantini, *Adv. Energy Mater.*, 2022, **12**, 2200412.

44 T. Hanemann and D. V. Szabó, *Materials*, 2010, **3**, 3468.

45 D. M. Correia, L. C. Fernandes, P. M. Martins, C. García-Astrain, C. M. Costa, J. Reguera and S. Lanceros-Méndez, *Adv. Funct. Mater.*, 2020, **30**, 1909736.

46 Y. Yang, H. Deng and Q. Fu, *Mater. Chem. Front.*, 2020, **4**, 3130–3152.

47 Z. He and P. Alexandridis, *Adv. Colloid Interface Sci.*, 2017, **244**, 54–70.

48 D. J. Wales, S. Miralles-Comins, I. Franco-Castillo, J. M. Cameron, Q. Cao, E. Karjalainen, J. Alves Fernandes, G. N. Newton, S. G. Mitchell and V. Sans, *Biomater. Sci.*, 2021, **9**, 5397–5406.

49 M. Jurinovs, A. Barkane, O. Platnieks, L. Grase and S. Gaidukovs, *ACS Appl. Polym. Mater.*, 2023, **5**(9), 7120–7131.

50 D. J. Wales, Q. Cao, K. Kastner, E. Karjalainen, G. N. Newton and V. Sans, *Adv. Mater.*, 2018, **30**, 1800159.

51 S. Miralles-Comins, M. Zanatta, A. F. Gualdrón-Reyes, J. Rodriguez-Pereira and V. Sans, *Nanoscale*, 2023, **15**, 4962–4971.

52 S. Sevilia, M. Yong, D. Grinstein, L. Gottlieb and Y. Eichen, *Macromol. Mater. Eng.*, 2019, **304**, 1900018.

53 S. Lee, M. D. Cummins, G. A. Willing and M. A. Firestone, *J. Mater. Chem.*, 2009, **19**, 8092–8101.

54 S. García-Garabal, M. Domínguez-Pérez, O. Cabeza, Y. Arosa, L. M. Varela, C. Fernández-López, J. Pérez-Juste and I. Pastoriza-Santos, *J. Chem. Eng. Data*, 2021, **66**, 3028–3037.

55 S. Gupta, A. Singh and N. Matsumi, *ACS Omega*, 2019, **4**, 20923–20930.

56 T. Ishikawa, M. Kobayashi and A. Takahara, *ACS Appl. Mater. Interfaces*, 2010, **2**, 1120–1128.

57 W. Zhu, F. Liu and J. He, *J. Mech. Behav. Biomed. Mater.*, 2017, **74**, 176–182.

58 B. Ran, Z. Zhang, L. Yin, T. Hu, Z. Jiang, Q. Wang and Y. Li, *J. Coat. Technol. Res.*, 2018, **15**, 345–349.

59 R. Carmenini, A. S. de León, M. C. Franchini, S. I. Molina and M. Matur, *Appl. Mater. Today*, 2026, 103018.

60 Z. Zhang, R. Krishna, E. S. Zofchak, N. Marioni, H. S. Sachar and V. Ganesan, *J. Chem. Phys.*, 2023, **159**, 084902.

61 H. Chen, J. H. Choi, D. S. D. La Cruz, K. I. Winey and Y. A. Elabd, *Macromolecules*, 2009, **42**, 4809–4816.

62 E. Ennis and S. T. Handy, *Curr. Org. Synth.*, 2007, **4**, 381–389.

63 E. Ennis and S. T. Handy, *Molecules*, 2009, **14**, 2235–2245.

64 M. Štaffová, F. Ondreáš, J. Svatík, M. Zbončák, J. Jančář and P. Lepcio, *Polym. Test.*, 2022, **108**, 107499.

65 L. Kool, A. Bunschoten, A. H. Velders and V. Saggiomo, *Beilstein J. Nanotechnol.*, 2019, **10**, 442.

66 W. Di Cianni, M. de la Mata, F. J. Delgado, J. Hernández-Saz, M. Herrera, S. I. Molina, M. Giocondo and A. S. de León, *Polym. Test.*, 2023, **117**, 107869.

67 F. M. Collares, F. F. Portella, V. C. B. Leitune and S. M. Werner-Samuel, *Braz. Oral Res.*, 2013, **27**, 453–454.

68 A. N. H. S. Delgado and A. M. Young, *PLoS One*, 2021, **16**(6), e0252999.

69 P. Pillai and A. Mandal, *Sep. Sci. Technol.*, 2020, **302**, 112553.

70 P. Navarro, M. Larriba, E. Rojo, J. García and F. Rodríguez, *J. Chem. Eng. Data*, 2013, **58**, 2187–2193.

71 M. Ferriol, A. Gentilhomme, M. Cochez, N. Oget and J. L. Mieloszynski, *Polym. Degrad. Stab.*, 2003, **79**, 271–281.

72 A. Laachachi, M. Cochez, M. Ferriol, J. M. Lopez-Cuesta and E. Leroy, *Mater. Lett.*, 2005, **59**, 36–39.

73 B. Demir, K.-Y. Chan, D. Yang, A. Mouritz, H. Lin, B. Jia, K.-T. Lau and T. R. Walsh, *Compos. Sci. Technol.*, 2019, **174**, 106–116.

74 S. C. Hamm, S. Basuray, S. Mukherjee, S. Sengupta, J. C. Mathai, G. A. Baker and S. Gangopadhyay, *J. Mater. Chem. A*, 2014, **2**, 792–803.

75 T. Hanemann and D. V. Szabó, *Materials*, 2010, **3**, 3468–3517.

76 Y. Zare, *Composites, Part A*, 2016, **84**, 158–164.

77 N. S. Allen, M. Edge and S. Hussain, *Polym. Degrad. Stab.*, 2022, **201**, 109977.

78 O. Ejeromedoghene, O. Oderinde and S. Adewuyi, *Phys. Sci. Rev.*, 2022, **7**, 759–772.